energies

MDPI

Article

A Dual-Mode Hybrid Step-Up Converter with Stable Output for Vibration Energy Harvesting

Jiayong Yuan [1], Han Peng [1,*], Jiahua Chen [1], Hanyi Sun [2] and Chunyan Zang [1]

[1] State Key Laboratory of Advanced Electromagnetic Engineering and Technology, School of Electrical and Electronic Engineering, Huazhong University of Science and Technology, Wuhan 430074, China; m202071578@hust.edu.cn (J.Y.); jhchen@hust.edu.cn (J.C.); zcy_peace@hust.edu.cn (C.Z.)

[2] China-EU Institute for Clean and Renewable Energy, Huazhong University of Science and Technology, Wuhan 430074, China; sunhy@hust.edu.cn

* Correspondence: pengh@hust.edu.cn

Abstract: A dual-mode hybrid step-up circuit for electromagnetic energy harvesting (EVEH) is proposed in this paper, with the merits of continuous output power delivery with and without external vibrations, simple architecture, and no need for extra circuits to start up. The proposed hybrid converter combines a multi-stage voltage multiplier (VM) with a boost regulator, which utilizes the winding inductance of the electromagnetic energy harvester as a boost inductor. With external vibration, the proposed circuit powers the load and stores energy in the super-capacitor through VM mode. When external vibration disappears, it automatically switches to boost mode and powers the load using the energy stored in the supercapacitor. For hybrid mode operation, the number of VM stages is optimized considering the following three aspects: sufficient voltage gains when vibration is on, time durations to provide constant power when vibration is off for as long as possible, and low losses at VM stage. A GaN-based dual-mode hybrid converter is built to verify the output regulation capability with an in-house-designed electromagnetic energy harvester. The outputs of the hybrid circuit achieve 4.05 V and 1.64 mW at a 100-Hz external vibration frequency and an acceleration of 0.7 g. The peak efficiency of the proposed hybrid converter reaches 60.7%. When external vibration disappears, the circuit is able to maintain a stable output for 13 s with a super-capacitor of 0.1 F.

Keywords: electromagnetic vibration energy harvesting; voltage multiplier; AC~DC converter; step-up converter; super-capacitor; hybrid dual-mode

Citation: Yuan, J.; Peng, H.; Chen, J.; Sun, H.; Zang, C. A Dual-Mode Hybrid Step-Up Converter with Stable Output for Vibration Energy Harvesting. *Energies* **2022**, *15*, 4643. https://doi.org/10.3390/en15134643

Academic Editors: Nick Papanikolaou and Anastasios Kyritsis

Received: 30 May 2022
Accepted: 20 June 2022
Published: 24 June 2022

1. Introduction

With the development of the Internet of Things (IOT), the demand for wireless sensors is increasing. Traditional battery-powered sensors can hardly ensure continuous operation and a long lifetime in remote areas and harsh environments [1]. Energy harvesting is a technology which harvests and converts the energy from the environment to electricity in order to power low-voltage electronic devices [2–5]. With the power requirement of sensors being reduced to sub-milli- to micro-watts, EH has become a promising technology to replace batteries, with the advantages of a long lifetime, being free of maintenance, and environmental friendliness.

Vibration, one of the most widely distributed energies in the environment, has become a premium energy source for EH [6]. With the merits of high output power and low cost, electromagnetic vibration energy harvesting (EVEH) has been widely adopted. According to the Faraday law of electromagnetic induction, the magnetic flux in the coil of EVEH changes and results in induced electromotive force. Figure 1 depicts the basic architecture of EVEH, which is composed of an energy harvester, an energy converter and an energy storage module. The energy harvester can be modeled as a voltage source $v_i(t)$ in series

with equivalent resistance R_{EH} and inductance L_{EH}. An energy converter is required to regulate the low-voltage AC to DC level.

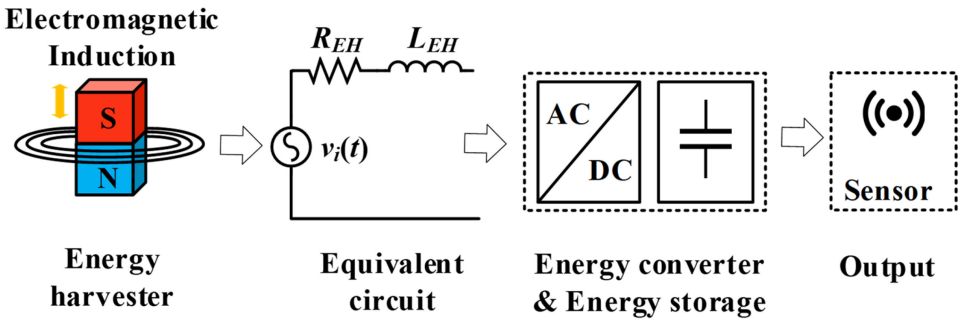

Figure 1. Basic architecture of electromagnetic EVEH.

Vibration energy in the environment has a wide dynamic range of frequencies and amplitudes. For example, the vibration of the bridge is related to its traffic flow [7], with an average vibration frequency of around 40 Hz and a peak frequency of up to 500 Hz when two vehicles meet oppositely side-by-side [8]. A conventional energy harvester is usually narrow banded, with one resonant frequency for maximum power harvesting [9]. When the vibration frequency deviates from the resonant frequency of EVEH, the ability to harvest energy will decrease significantly, which lead to no or very little output power. Therefore, energy storage is necessary to provide energy to the output when the vibration fluctuates or disappears.

However, some existing works did not include a storage element [10–12]. Existing converters with energy storages were relatively complex in circuit topology and control strategy while ensuring stable output. Although an energy storage component was included in [13,14], it was directly applied to power the load when vibration disappears. Such a configuration failed to maintain a stable voltage for the sensors, which leads to increased power consumptions or the degradation of the sensors' performances [15]. In order to maintain a stable output voltage level when vibration disappears, the voltage level of energy storage component needs to be regulated before sending it to the load. As shown in Figure 2, the energy storage module acted as an intermediate DC bus, and an additional DC-DC converter was employed to power the load [16–18]. Another typical approach is the three-port converter, as depicted in Figure 3 [19,20]. Both the energy storage component and load are charged by the vibration source once it exists. When the vibration disappears, the energy storage component will become the power source for the load through the AC-DC converter. Such architectures and their control strategies are complex and high cost.

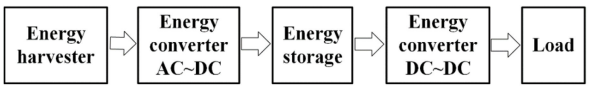

Figure 2. The energy storage module as the intermediate bus voltage in the EH system [16–18].

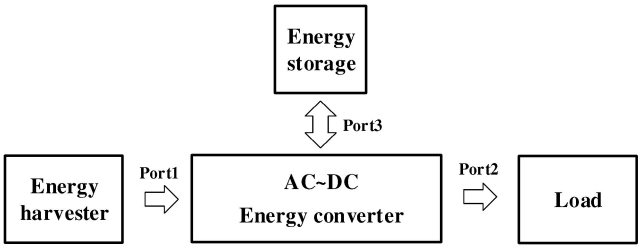

Figure 3. A three-port power converter for EH, with the energy storage module as one port [19,20].

In our previous work [21], a new dual-mode hybrid step-up converter was proposed with dual-mode operation to realize the resistance of the input vibration disturbance in

a simple architecture. However, a converter based on a double-voltage circuit cannot achieve satisfactory output when the input voltage is low. In order to expand the range of input voltage, a converter based on a multiple-voltage circuit is proposed on the basis of [21], as shown in Figure 4. The converter merges the voltage multiplier (VM) and boost regulator, and utilizes the super-capacitor as the energy storage module. When vibration exists, the hybrid converter works in VM mode to power the load and store energy in the supercapacitor. When vibration disappears, the output is powered through the energy stored in the supercapacitor, and the hybrid converter is switched to boost mode. Furthermore, the proposed converter will start working once the output of the EVEH is higher than the forward voltage drop of the diodes and no extra start-up circuits are required [12,19].

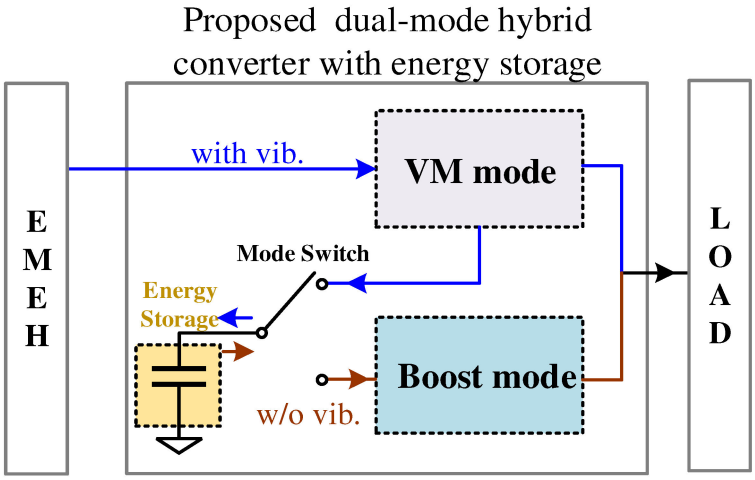

Figure 4. System architecture of the proposed dual-mode hybrid converter.

The organization of the rest of the paper is as follows: Section 2 discusses the structure and working process of the proposed converter. Section 3 analyzes the output characteristics. Control strategies are provided briefly in Section 4. Section 5 explores the design principles of the proposed circuit, including the selection of the number of stages and the super-capacitor, loss analysis, targeting at sufficient voltage amplification at VM mode, and long operation duration in boost mode. The measurement results are further given in Section 6. Finally, conclusions are drawn in Section 7.

2. System Architecture and Mode Control

Figure 5 shows the full schematic of the proposed dual-mode hybrid VM-boost converter, which consists of the main power stage, the mode switching circuit and the PWM regulation module. A low-dropout regulator (LDO) is used to further stabilize the output level. The main power stage is a n-stages VM with boost mode merged with the first stage of VM, where the winding inductance from the electromagnetic energy harvester is adopted as the boost inductor. C_1 is a large super-capacitor for energy storage and serves as an energy source when vibration disappears. The mode switching circuit determines the VM and boost operation modes for the proposed converter.

The reference voltages used in the circuit follow the relationship $V_{O\_VM} > V_{hys+} > V_{com} > V_{O\_boost} = V_{ref} > V_{hys-}$. V_{O_VM} and V_{O_boost} represent the output for VM mode and boost mode, respectively. Under VM mode, U_1 is shut down by setting the *sd* terminal at a low level. When the output falls below V_{com} because of the disappearance of vibration, the converter will switch to boost mode with the *sd* terminal enabled. The output voltage is controlled by the PWM regulation module with V_{ref} in boost mode. V_{hys+} is used to ensure that C_1 is pre-charged first by VM mode. Otherwise, boost mode will be enabled at the system's start-up transient. As soon as the voltage level in C_1 is dropped below V_{hys-}, the converter will stop boost mode operation, and the system is shut down where there is

insufficient energy in C_1 to meet the load requirement. The mode control strategies and key operation waveforms of the proposed converter are summarized in Figure 6.

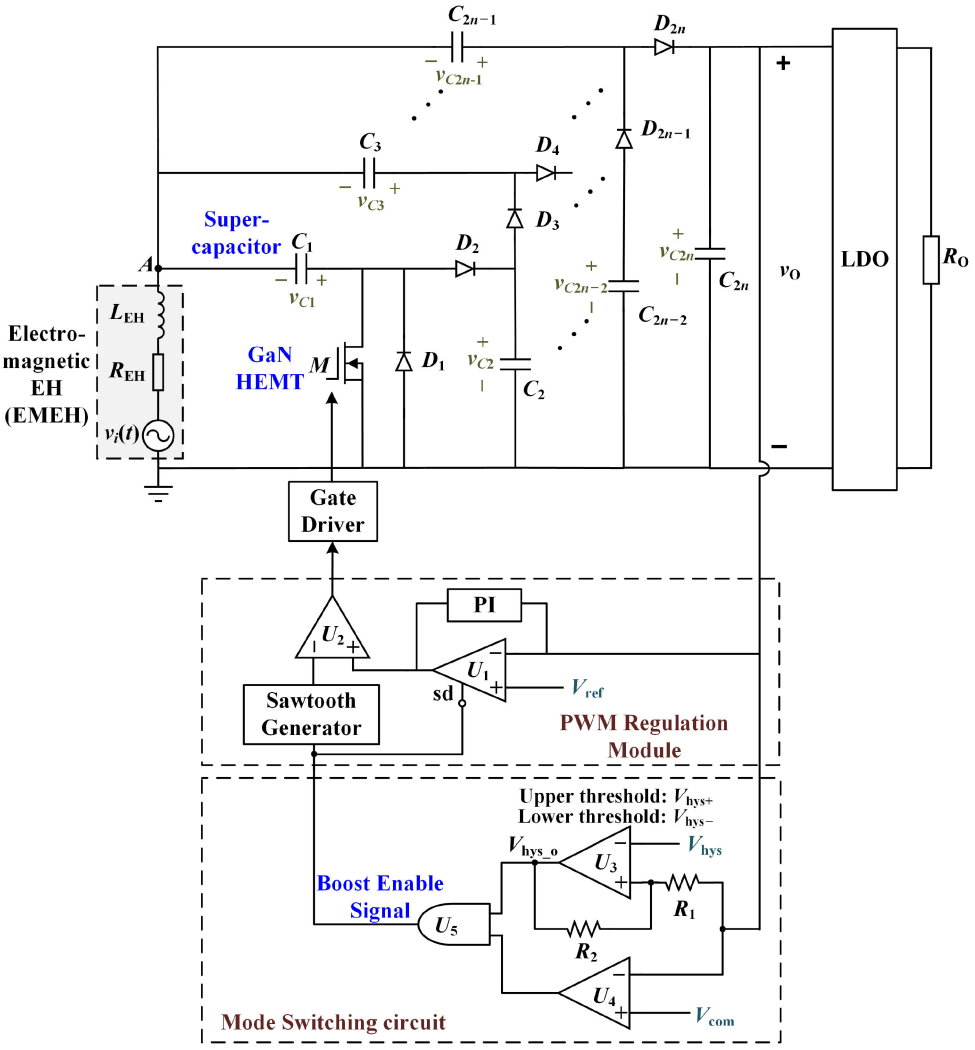

Figure 5. The full schematic of the proposed hybrid VM–boost converter.

t_0–t_1: At t_0, the vibration appears and the converter starts to work in VM mode. v_O will gradually rise to the stabilized value of V_{O_VM}.

t_1–t_2: The vibration disappears at t_1. VM mode stops and v_O begins to drop according to the load requirement.

t_2–t_3: v_O drops to V_{com} at t_2 and the hybrid converter will switch to boost mode. The load will be powered by C_1. The output is regulated to V_{O_boost} and the voltage of the C_1 drops gradually.

t_3–t_4: Vibration resumes at t_3, and v_O begins to rise above V_{O_boost}. However, v_O is still lower than V_{com} in this period, such that the boost mode is not disabled. The hybrid converter operates with the coexistence of VM mode and boost mode.

t_4–t_5: v_O rises above V_{com} at t_4 and the converter starts to work in VM mode. v_O will be maintained at V_{O_VM}.

t_5–t_6: Vibration disappears at t_5. This interval is the same as [t_1–t_2].

t_6–t_7: v_O drops to V_{com} at t_6 and the hybrid converter will switch to boost mode. This interval is the same as [t_2–t_3]. The time duration for which the converter is able to provide a stable output is defined as t_{boost}.

t_7–t_8: At t_7, the energy stored in C_1 is not enough to maintain the output at V_{O_boost}. Although the converter is still in boost mode, v_O will decrease from V_{O_boost}.

***t*8−:** When v_O drops to V_{hys-} at t_8, the system is shut down. The output voltage and the voltage across C_1 will gradually drop to zero. If the vibration resumes, the process starting from t_0 is repeated.

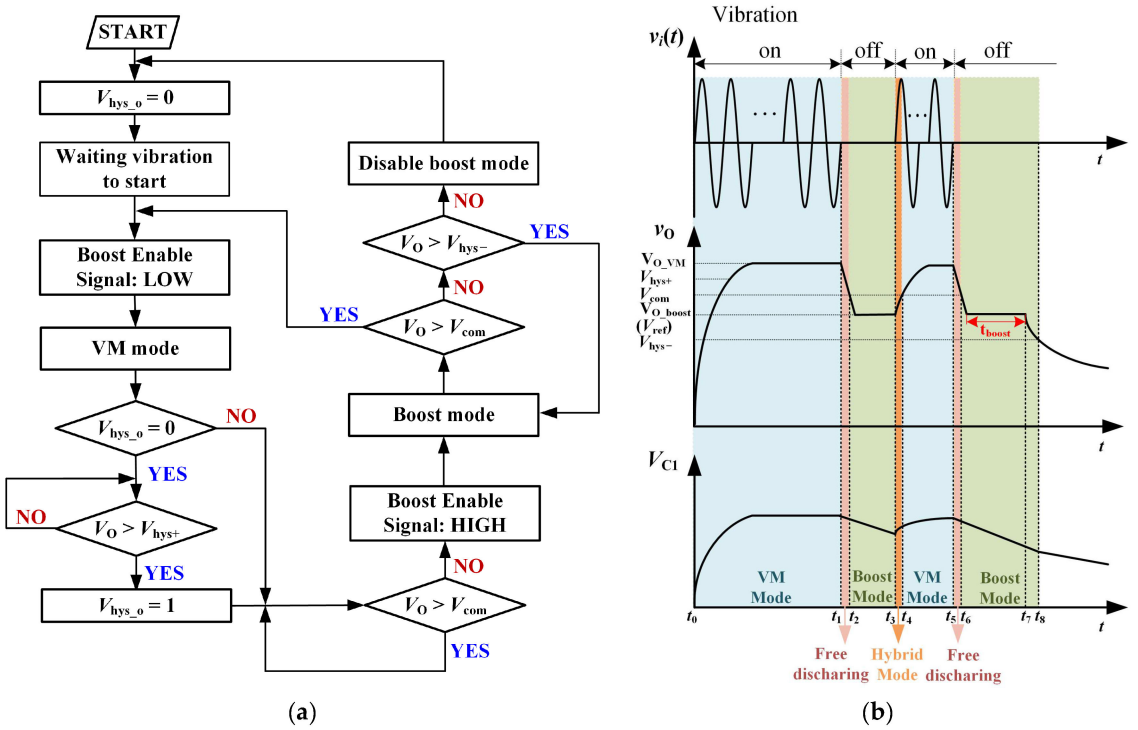

Figure 6. (**a**) The flow chart of the proposed dual-mode hybrid converter; (**b**) key waveforms of the proposed converter with vibration on (existing) and off (disappearing).

3. Output Characteristics

As shown in Figure 5, the converter works in the VM mode and the main power transistor M is off when vibration exists. When $v_i(t)$ is negative, $v_i(t)$ and $C_{2i(i=1,2\ldots n-1)}$ charge the capacitor $C_{2i+1(i=1,2\ldots n-1)}$ through $D_{2i+1(i=1,2\ldots n-1)}$. According to Kirchhoff's voltage law (KVL) and the law of the conservation of electric charge (CEC), the capacitors' voltage in this interval can be expressed as

$$\begin{gathered} V_{C1}^{-} = V_p - V_D - I_{VM\_avg}R_{EH} \\ V_{C2i-1(i=2,3\ldots n)}^{-} = V_{C2i-2(i=2,3\ldots n)}^{-} + V_p - V_D - I_{VM\_avg}R_{EH} \\ V_{C2i(i=1,2\ldots n)}^{-} = V_{C2i(i=1,2\ldots n)}^{+} - \frac{\Delta Q_{VM}}{C_{2i(i=1,2\ldots n)}} \end{gathered} \tag{1}$$

where R_O is the load of the converter, and f_{vib} is the frequency of vibration. V_p is the peak amplitude of $v_i(t)$, and V_D is the forward voltage drop of the diodes. ΔQ_{VM} is the transferred charge in one vibration period, and satisfies $\Delta Q_{VM} = V_{O\_VM}/(R_O f_{vib})$. I_{VM_avg} is the average current of $v_i(t)$.

When $v_i(t)$ is positive, $v_i(t)$ and the capacitor $C_{2i-1(i=1,2\ldots n)}$ provide energy to $C_{2i(i=1,2\ldots n)}$ through $D_{2i(i=1,2\ldots n)}$. According to KVL and CEC, the capacitors' voltage in this interval can be expressed as

$$\begin{gathered} V_{C2i(i=1,2\ldots n)}^{+} = V_{C2i-1(i=1,2\ldots n)}^{+} + V_p - V_D - I_{VM\_avg}R_{EH} \\ V_{C2i-1(i=1,2\ldots n)}^{+} = V_{C2i-1(i=1,2\ldots n)}^{-} - \frac{\Delta Q_{VM}}{C_{2i-1(i=1,2\ldots n)}} \end{gathered} \tag{2}$$

By combining (1) and (2), the output of VM mode can be derived by charge conservation as

$$V_{O\_VM} = V_{C2n} = \frac{V_{C2n}^{-} + V_{C2n}^{+}}{2} = \frac{2n(V_p - V_D)}{1 + \frac{4n^2 R_{EH}}{R_O} + \frac{X_{C\_vib}}{R_O}} \tag{3}$$

where $X_{C\_vib} = \frac{1}{f_{vib}}\left(\sum_{i=1}^{2n-1}\frac{1}{C_i} + \frac{1}{2C_{2n}}\right)$. According to CEC, $I_{VM\_avg} = 2nI_O = 2nV_{O\_VM}/R_L$. According to (1), the voltage over super-capacitor C_1 is charged to:

$$V_{C1} = \frac{(V_p - V_D)(X_{C\_vib} + R_O)}{4n^2R_{EH} + X_{C\_vib} + R_O} \tag{4}$$

When vibration disappears, the converter will switch to boost mode and the energy stored in C_1 starts to discharge in order to provide power to the output. Figure 7 shows the equivalent circuits and charge flow paths when M is off and on in one switching cycle. A constant current source (I_O) is used as the load. ΔQ_{Boost} represents the transferred charge in one switching period, and satisfies $\Delta Q_{Boost} = I_O/f_s$, where f_s is the switching frequency in boost mode.

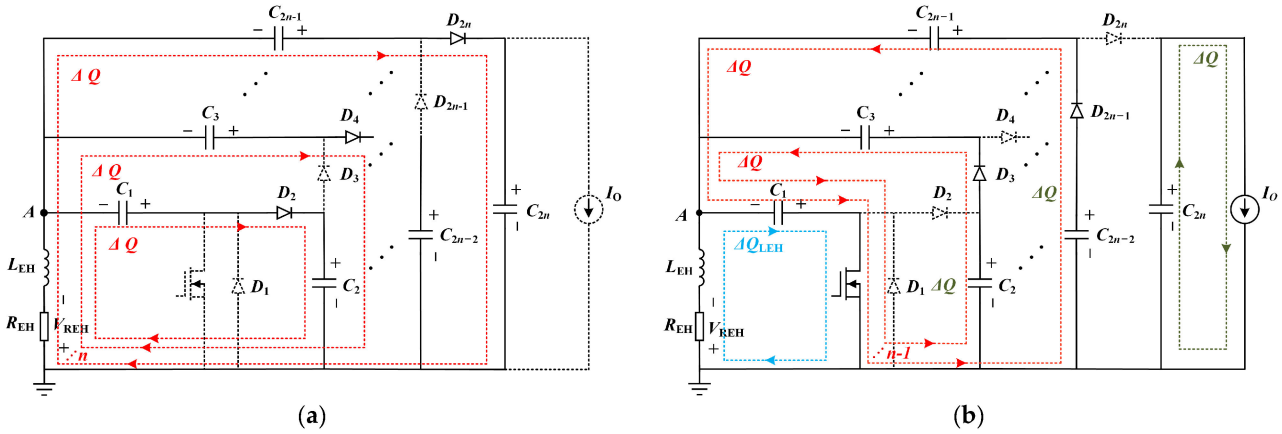

Figure 7. (**a**) The charge flow when M is off in boost mode; (**b**) the charge flow when M is on in boost mode.

When M turns off in the $(1 - D)\ T_s$ interval, as shown in Figure 7a, C_1 and L_{EH} charge C_2 through D_2 with ΔQ_{Boost} transferred, where D is the duty ratio of boost mode. Simultaneously, C_3 and L_{EH} charge C_4 through D_4 with ΔQ_{Boost} transferred, as do $C_{2i-1(i=1,2\ldots n)}$ and L_{EH}. Therefore, the total charge dissipated from L_{EH} becomes $n\Delta Q_{Boost}$. Assuming that the inductor current is continuous, the average inductor current can be expressed as: $I_{L\_avg} = n\Delta Q_{Boost}f_s/(1 - D)$. As such, the voltage drop across R_{EH} is $V_{REH} = I_{L\_avg} \times R_{EH} = nI_OR_{EH}/(1 - D)$. Furthermore, the voltage of the L_{EH} can be derived using volt-second balance. According to KVL and CEC, the capacitors' voltage in this interval can be expressed as

$$v^{M\_off}_{C2i(i=1,2\ldots n)} = v^{M\_off}_{C2i-1(i=1,2\ldots n)} + v^{M\_off}_{A} - V_D \tag{5}$$

$$v^{M\_off}_{C2i-1(i=2,3\ldots n)} = v^{M\_on}_{C2i-1(i=2,3\ldots n)} - \frac{\Delta Q_{Boost}}{C_{2i-1(i=2,3\ldots n)}} \tag{6}$$

where $v^{M\_off}_{A}$ is the voltage across L_{EH} and R_{EH} when M is off.

As shown in Figure 7a, when M is on in the DT_s interval, C_1 charges L_{EH} with ΔQ_{LEH}. Simultaneously, C_1 and C_2 charge C_3 through D_3 with ΔQ_{Boost}, and C_1 and C_4 charge C_5 through D_5 with ΔQ_{Boost}, as do C_1 and $C_{2i-2(i=2,3\ldots n)}$. Hence, ΔQ_{LEH} equals to $n\Delta Q_{Boost}D/(1 - D)$. According to KVL and CEC, the capacitors' voltage in this interval can be expressed as

$$v^{M\_on}_{C2i-1(i=2,3\ldots n)} = v^{M\_off}_{C2i-2(i=2,3\ldots n)} - v^{M\_on}_{A} - V_D \tag{7}$$

$$v^{M\_on}_{C2i(i=1,2\ldots n)} = v^{M\_off}_{C2i(i=1,2\ldots n)} - \frac{\Delta Q_{Boost}}{C_{2i(i=1,2\ldots n)}} \tag{8}$$

where $v^{M\_on}_{A}$ is the voltage across L_{EH} and R_{EH} when M is on.

Assuming that the voltage across C_1 does not change in one switching period—e.g., $v_{C1}^{M\_on} = v_{C1}^{M\_off} = V_{C1}$—$V_{O\_boost}$ can be expressed according to (5)–(8):

$$V_{O\_boost} = \frac{v_{2n}^{M\_on} + v_{2n}^{M\_off}}{2} = \frac{n\frac{V_{C1}}{1-D} - (2n-1)V_D}{1 + \frac{n^2 R_{EH}}{R_O(1-D)^2} + \frac{X_{C\_s}}{R_O}} \tag{9}$$

where $X_{C\_s} = \frac{1}{f_s}\left(\sum_{i=1}^{2n-1}\frac{1}{C_i} + \frac{1}{2C_{2n}}\right)$.

4. PWM Regulation for Boost Mode

A PI-based PWM regulation is adopted for output control under boost mode, as shown in Figures 8 and 9. The PI output is compared with the sawtooth wave (V_{saw}) to generate the PWM signal for the gate driver of GaN HEMT devices (M). The sawtooth generator is composed of series resistor R_s, capacitor C_s, two voltage comparators, a RS trigger, and switch S_2, as shown in Figure 9. The two voltage thresholds are set as V_{High} and V_{Low} ($V_{High} > V_{Low}$). If V_{saw} is higher than V_{High} or lower than V_{Low}, the status of the RS trigger changes to control the on and off of S_2. According to the RC charging theorem, the frequency of the sawtooth wave can be expressed as

$$f_s = \frac{1}{R_s C_s \ln\frac{V_{CC}-V_{Low}}{V_{CC}-V_{High}}} \tag{10}$$

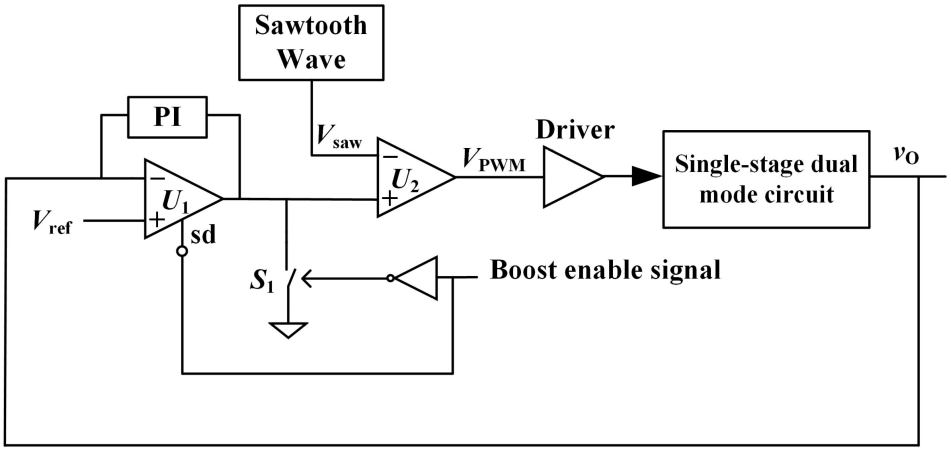

Figure 8. PI-regulated boost mode operation.

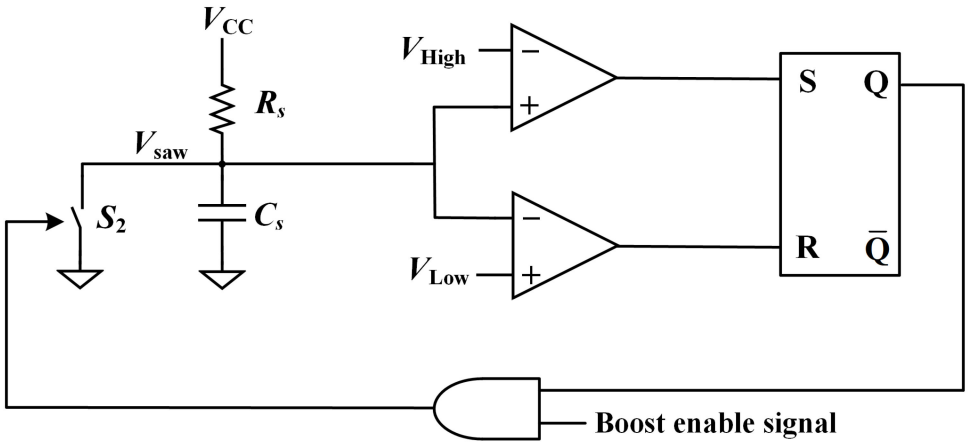

Figure 9. The sawtooth wave generation circuit.

To avoid the mode oscillations during mode switch, S_1 is closed in order to maintain the output of the PI regulator at a low level under VM mode, as shown in Figure 8.

5. Key Parameters and Analysis

As can be seen from (3) and (9), the output voltage of the proposed hybrid converter is dependent on the number of stages and the design of the super-capacitor. In order to realize sufficient voltage amplification at VM mode and ensure a long operation duration (t_{boost}) in boost mode, these two parameters are fully studied in this section. In the meantime, the loss distributions of VM mode are analyzed, which also leads to the optimum design of the number of VM stages.

5.1. Selection of the Number of Stages

For VM mode, the VM converter needs to tolerate the variations of the load resistors (R_O) and R_{EH}. Assuming that $C_1 = C_2 = \ldots = C_{2n} = C$, the minimum required number of stages can be derived through (3), as

$$n_{min} = \frac{-V_{O\_VM} + \frac{R_O}{X}(V_p - V_D) \pm \sqrt{(\frac{R_{EH}}{X})^2 (V_p - V_D)^2 + 2\frac{R_O}{X} V_{O\_VM}(V_p - V_D) + V_{O\_VM}^2[(4 - 4\frac{R_O}{X} - 2\frac{C_i}{C_{2n}})\frac{R_{EH}}{X} + 1]}}{4\frac{R_{EH}}{X} V_{O\_VM}} \quad (11)$$

where $X = \frac{1}{Cf_{vib}}$.

V_{O_VM} increases first, then decreases with the increase of the number of stages. n_{max} is defined as the number of stages when the output voltage reaches its maximum value under a certain input. The n_{max} for the peak output voltage at a certain load resistor can be deduced from $dV_{O\_VM}/dn = 0$, as

$$n_{max} = \frac{\sqrt{2C_{2n}\frac{R_{EH}}{X}(2C_{2n}\frac{R_O}{X} + C_i - 2C_{2n})}}{4C_{2n}\frac{R_{EH}}{X}} \quad (12)$$

Hence, with an LDO post-regulation, the possible number of stages for a certain V_{O_VM} should be chosen as

$$n_{min} \leq n \leq n_{max} \quad (13)$$

Figure 10a describes the relationship between the number of stages and V_{O_VM} with different R_O at an R_{EH} of 100 Ω. The higher R_O is, the smaller the number of stages required for a certain V_{O_VM}. Figure 10b describes the relationship between the number of stages and V_{O_VM} with different R_{EH} at R_O of 10 kΩ. The higher R_{EH} is, the larger the number of stages required for a certain V_{O_VM}. According to (1), the minimum R_O for a certain output V_{O_VM} can be derived as

$$R_{O(min)} = \frac{V_{O\_VM}(4R_{EH}n^2 + X_{C\_vib})}{2n(V_p - V_D) - V_{O\_VM}} \quad (14)$$

If $R_O \leq R_{O(min)}$, the converter can't stabilize to V_{O_VM}. If the load $R_O > R_{O(min)}$, the LDO module is required to further stabilize the output to V_{O_VM}.

For boost mode, the main target is to provide a stable output as long as possible when vibration disappears. Considering that C_1 reaches a steady state before vibration disappears, the total energy stored in C_1 will be divided into three parts in boost mode, as shown in Figure 11: E_{load} is the energy transferred to the output; E_{loss} is the energy dissipated in the circuit, and E_{left} represents the energy leftover in C_1 when the output fails to be regulated to V_{O_boost}. Therefore, $E_{total\_C1} = E_{left} + E_{load} + E_{loss}$. In order to extend the duration for a stable output when vibration disappears, E_{total_C1} should be large and the proportion of E_{load} should be as large as possible for a certain E_{total_C1}.

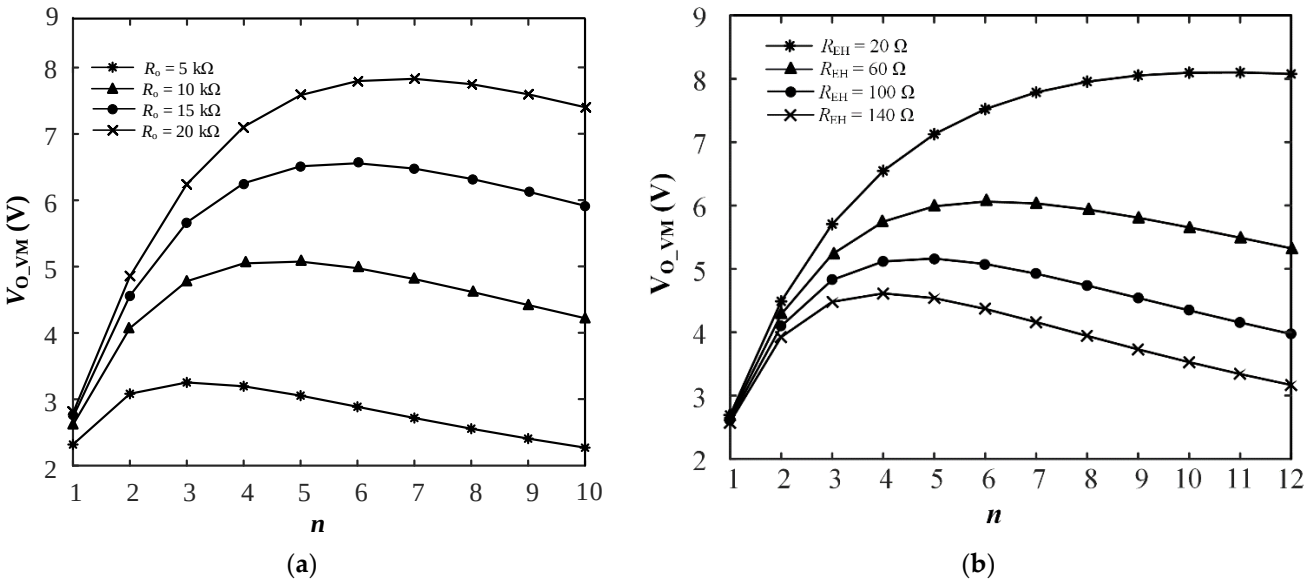

Figure 10. (**a**) The relationship of n and V_{O_VM} at different load resistors with R_{EH} = 100 Ω; (**b**) the relationship of n and V_{O_VM} at different EH output resistors with R_O = 10 kΩ.

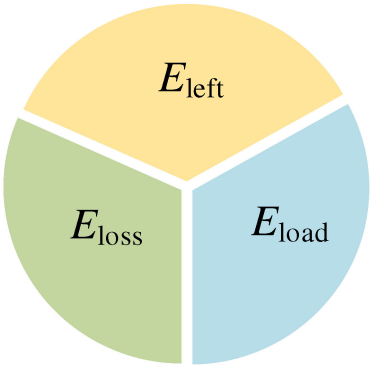

Figure 11. The distribution of energy stored in the super-capacitor in boost mode.

The initial voltage across the super-capacitor C_1 in boost mode (V_{C1_max}) can be derived by (4). The larger V_{C1_max} is, the larger E_{total_C1} will be. V_{C1_max} decreases with the increase of n.

When the converter operates at maximum duty cycle D_{max}, C_1 reaches to its minimum voltage level to be capable to provide a well-regulated V_{O_boost}. D_{max} can be obtained by forcing $dV_{O\_boost}/dD = 0$. Therefore, the minimum V_{C1} to maintain V_{O_boost} becomes:

$$V_{C1\_min} = \frac{2\sqrt{R_{EH}V_{O\_boost}(R_O V_{O\_boost} - R_O V_D + X_{C\_s}V_{O\_boost} + 2nR_O V_D)}}{R_O} \quad (15)$$

The lower V_{C1_min} is, the lower E_{left} will be. As V_{C1_min} increases with the increase of n, the more number of stages adopted, the more proportion of E_{left} will be.

The total transferred charge of C_1 (Q_{C1_output}) is directly related with E_{load} + E_{loss} in one boost period, as

$$Q_{C1\_output} = [(n-1)\Delta Q + \Delta Q]f_s t_{boost} + \int_0^{t_{boost}} \Delta Q_{LEH} f_s dt = nI_O t_{boost} + nI_O \int_0^{t_{boost}} \frac{D(t)}{1-D(t)} dt \quad (16)$$

It can be seen that the more number of stages will be, the more charges are required from C_1 to power the output for a certain t_{boost} under the same load and output voltage. It

can be concluded that E_{load} is reversely proportional to the number of stages under certain E_{total_C1}. Hence, combing the two aspects for both with (VM mode) and without (Boost mode) vibration, the minimum feasible number of stages (n_{min}) should be selected.

5.2. Design of Super-Capacitor C_1

In order to ensure that the selected C_1 can provide sufficient energy during required t_{boost} time interval, C_1 is designed under the most extreme condition where maximum duty ratio is always applied. It is the situation when the discharge rate of C_1 is highest. According to (16), C_1 can be chosen as

$$C_1 = \frac{nI_O t_{boost}(1 + \frac{D_{max}}{1-D_{max}})}{V_{C1\_max} - V_{C1\_min}} \tag{17}$$

5.3. Loss Analysis

As the VM mode is the main circuit processing EH power, the power consumptions of VM mode are discussed in this section. In EVEH, R_{EH} is usually much larger than the impedance of winding inductance of $j\omega L_{EH}$, so that L_{EH} is ignored the loss analysis. The charging current of capacitor is shown in Figure 12, where $I_{VM}(t)$ is the current of EH source. Capacitors are only charged during the intervals of t_1~t_2 and ($T - t_2$~$T - t_1$) in one vibration period.

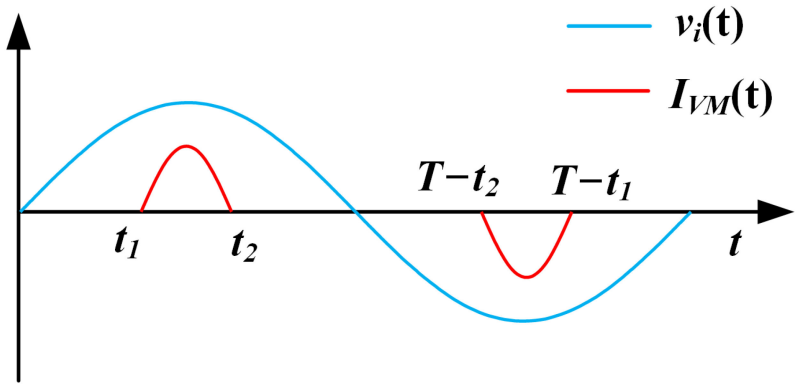

Figure 12. The current and voltage waveforms of source when vibration exists.

In negative half period, odd number capacitors $C_{2i-1(i=1,2\ldots n)}$ in Figure 5 are charged by EH source with the following relationships satisfied:

$$V_p \sin(2\pi f_{vib} t) - V_D - I_{VM}(t)R_{EH} > V_{C1} V_p \sin(2\pi f_{vib} t) - V_D - I_{VM}(t)R_{EH} > V_{C2i-1(i=2\ldots n)} - V_{C2i-2(i=2\ldots n)} \tag{18}$$

In positive half period, even number capacitors $C_{2i(i=1,2\ldots n)}$ in Figure 5 are charged with the following formula satisfied:

$$V_p \sin(2\pi f_{vib} t) - V_D - I_{VM}(t)R_{EH} > V_{C2} - V_{C1} V_p \sin(2\pi f_{vib} t) - V_D - I_{VM}(t)R_{EH} > V_{C2i(i=2\ldots n)} - V_{C2i-1(i=1,2\ldots n)} \tag{19}$$

Ignoring the voltage variations in C_1 as it is quite large, $I_{VM}(t)$ can be calculated as

$$I_{VM}(t) = \begin{cases} \frac{V_p \sin(2\pi f_{vib} t) - V_D - V_{C1}}{R_{EH}} & t \in (t_1 \sim t_2) \\ -\frac{V_p \sin(2\pi f_{vib} t) - V_D - V_{C1}}{R_{EH}} & t \in (T - t_1 \sim T - t_2) \\ 0 & t \in other \end{cases} \tag{20}$$

where $t_1 = \frac{1}{2\pi f_{vib}} \sin^{-1}(\frac{V_{C1}+V_D}{V_P})$ and $t_2 = \frac{1}{2\pi f_{vib}}[\pi - \sin^{-1}(\frac{V_{C1}+V_D}{V_P})]$.

5.3.1. Loss of R_{EH}

R_{EH} is the output resistance of the EVEH source and its power loss can be expressed as

$$P_{loss\_REH} = 2f_{\mathrm{vib}} \int_{t_1}^{t_2} I_{\mathrm{VM}}^2(t) R_{EH} dt \tag{21}$$

5.3.2. Loss of Capacitors' Charge Transfer

When the charge ΔQ_{AB} is transferred from capacitor A (C_A) with initial voltage u_A to capacitor B (C_B) with initial voltage u_B, according to CEC, the loss of charge transfer is:

$$P_{loss\_CAB} = (u_A - u_B)\Delta Q_{AB} - \frac{1}{2}\Delta Q_{AB}^2 (\frac{1}{C_A} + \frac{1}{C_B}) \tag{22}$$

In each vibration period, ΔQ_{VM} is transferred between the $C_{i(i = 1,2 \ldots 2n)}$ and $C_{i+1(i = 1,2 \ldots 2n-1)}$. Assuming that $C_{i(i = 2 \ldots 2n)}$ is large enough with ignorable voltage ripples, the loss of $C_{i(i = 1,2 \ldots 2n)}$ in the process of charge transfer can be expressed as

$$P_{loss\_\sum C} = (2n-1) f_{\mathrm{vib}} \Delta Q_{VM} V_{C1} - \frac{1}{2} f_{\mathrm{vib}} \Delta Q_{\mathrm{VM}}^2 (2 \sum_{i=1}^{2n-1} \frac{1}{C_i} + \frac{1}{C_{2n}}) \tag{23}$$

5.3.3. Loss of Diodes

Diode $D_{i(i = 1,3 \ldots 2n-1)}$ and $D_{i(i = 2,4 \ldots 2n)}$ turns on during time intervals (t_1~t_2) and ($T - t_2$~$T - t_1$) respectively in each EM period. Hence, diodes' conduction losses can be described as

$$P_{loss\_Don} = 2n f_{\mathrm{vib}} \int_{t_1}^{t_2} \frac{I_{\mathrm{VM}}(t) V_D}{n} dt \tag{24}$$

When diodes are off, leakage current will also induce loss, as

$$P_{loss\_Doff} = 2n f_{\mathrm{vib}} I_{leak} \left\{ 2 \int_{t_2}^{T-t_2} [V_{C1} + V_p \sin(2\pi f_{\mathrm{vib}} t)] dt + (t_2 - t_1)[V_{C1} + V_p \sin(2\pi f_{\mathrm{vib}} t_1)] \right\} \tag{25}$$

where I_{leak} is the reverse leakage current of diodes. Therefore, the overall losses of diodes can be expressed as

$$P_{loss\_\sum D} = P_{loss\_Don} + P_{loss\_Doff} \tag{26}$$

5.3.4. Loss of Super-Capacitor

Super-capacitors have large series resistors in the order to tens of ohms. The power consumptions on the parasitic resistor (R_{C1}) can be expressed as

$$P_{loss\_R_{C1}} = 2f_{\mathrm{vib}} \int_{t_1}^{t_2} (\frac{I_{\mathrm{VM}}(t)}{n})^2 R_{C1} dt \tag{27}$$

In order to evaluate the loss contributions in the VM mode of the proposed circuit, the circuit parameters are given in Table 1. As shown in Figure 13, the charge transfer loss is the major loss contributor, which is 75.8% of the total losses. The second largest loss contributor is diode conduction loss, which accounts for 20.8% of the total losses. Both the charge transfer loss and diode conductor loss increase with the increase of the number of stages (n). The power losses on EVEH's internal resistor and parasitic resistor at the super capacitor are negligible. Therefore, the minimum number of stages to provide sufficient output voltage level should be used. This conclusion is also consistent with the discussions in Section 5.1.

Table 1. The circuit parameters of VM mode used in the loss analysis.

Name	Value	Name	Value
n	2	V_D	0.3 V
V_p	1.8 V	I_{leak}	0.05 mA
f_{vib}	100 Hz	R_{EH}	105 Ω
C_1	100 mF	R_{C1}	20 Ω
C_2, C_3	10 μF	R_{O}	10 kΩ
C_4	100 μF		

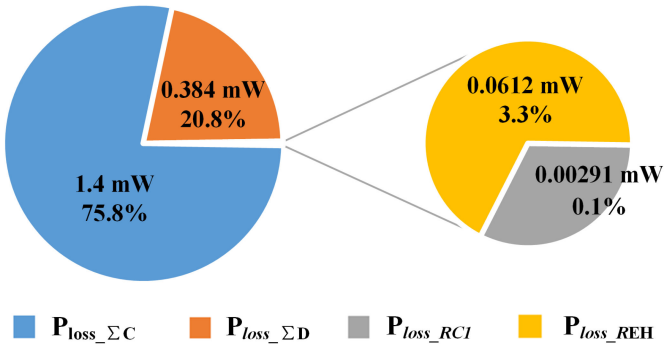

Figure 13. Power loss distributions of a two-stage VM circuit.

6. Prototype Design and Measurement Results

A cylindrical EVEH [22] is employed in this experiment as the source for the proposed dual-mode converter. As shown in Figure 14a, it is designed with a cylindrical magnet, two planar springs connected to the top and bottom of the magnet, and two sets of windings. The measured winding resistance R_{EH} and inductance L_{EH} are 105 Ω and 5.1 mH, respectively. The designed EVEH has a 4.2-cm height and a 2-cm diameter. At a vibration resonance frequency of 100 Hz and an acceleration of 0.7 g, the AC output amplitude (V_p) reaches 1.8 V. The prototype of the dual-mode hybrid step-up circuit is shown in Figure 14b. A Schokky diode (VS-10BQ015HM3) with a low forward conduction voltage of 0.3 V is used. A GaN HEMT EPC2015C (40 V/53 A) is employed as the main switching transistor. V_{com}, V_{hys}, $V_{\text{hys+}}$ and $V_{\text{hys−}}$ are set to 3.4 V, 2.25 V, 3.6 V and 0.6 V, respectively. V_{ref} for the boost mode output is set to 3.3 V. According to (11), the number of stages should be chosen as two. The key parameters used in this design are summarized in Table 2.

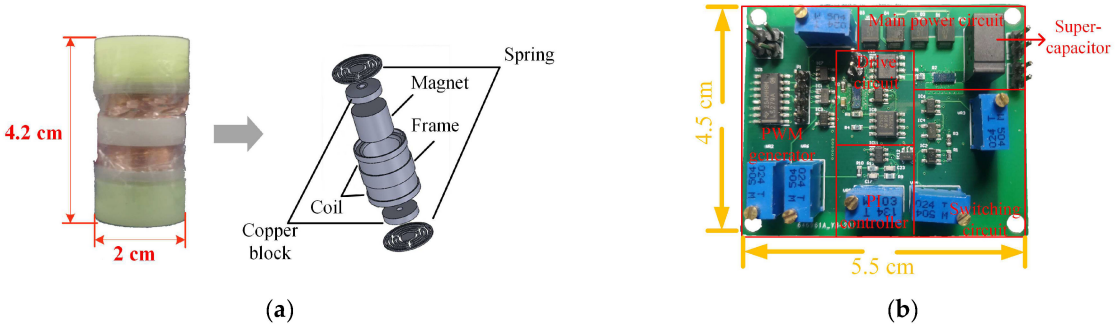

Figure 14. (**a**) The EVEH module used in the system [22]; (**b**) the prototype of the designed dual-mode hybrid step-up circuit.

Figure 15 shows the waveforms of VM mode operation under vibration. The output voltage of the VM circuit and voltage across the supercapacitor are maintained at 4.05 V and 1.23 V, respectively. Figure 16 shows the circuit efficiency (η) of the VM circuit when n = 2 with different load resistors and the same V_p, where the peak efficiency reaches 60.7%.

Table 2. The key components used in this design.

Name	Component	Value
R_O	Load	10 kΩ
C_1	Super-capacitor	FM0H104ZF (0.1 F)
C_2, C_3	Flying capacitors	10 μF
C_4	Filter capacitor	100 μF
$D_{i(i=1\sim4)}$	Schottky diode	VS-10BQ015HM3
M	N-channel GaN HEMT	EPC2015C
U_{driver}	Gate driver	UCC27525

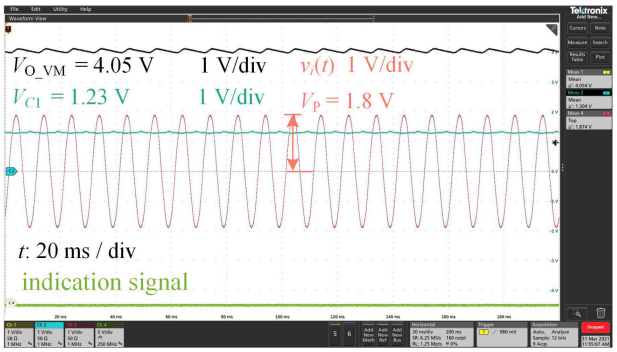

Figure 15. Steady state operation of VM mode under vibration with a vibration frequency of 100 Hz and an acceleration of 0.7 g.

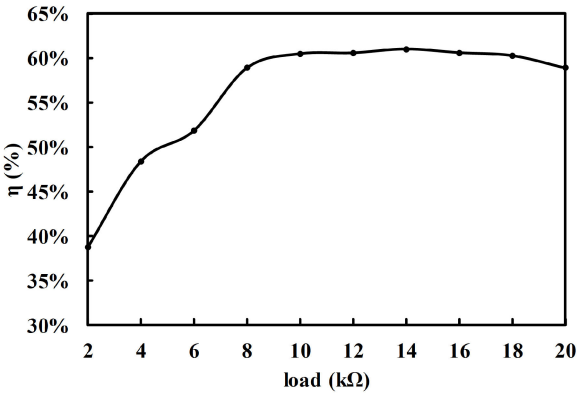

Figure 16. VM efficiency (η) at different load resistors with a vibration frequency of 100 Hz and V_p = 1.8 V.

Figure 17 reveals the different cases of the operation modes transitions from the existence (①) of vibration to the disappearance of vibration (②) and the resumption of vibration (③). Four different cases are studied:

Case 1: In Figure 17a, the vibration is resumed after 700 ms of disappearance. v_O is stabilized to 3.3 V during the disappearance period. V_{C1} drops to 1.19 V from 1.23 V. v_O and V_{C1} rise to 3.3 V and 1.23 V after vibration is resumed, respectively.

Case 2: In Figure 17b, the vibration is resumed after a 14.7-s disappearance. v_O is stabilized to V_{O_boost} (3.3 V), and V_{C1} drops to 1.0 V from 1.23 V in the first 13 s. After 13 s, the boost mode cannot keep v_O to V_{O_boost}, and v_O begins to decrease. At 14.7 s, v_O drops to 3 V and V_{C1} drops to 0.95 V. v_O and V_{C1} rise to 3.3 V and 1.23 V after vibration is resumed, respectively.

Case 3: As shown in Figure 17c, v_O is stabilized to 3.3 V for 13 s and drops after the vibration's disappearance. The vibration is resumed after a 24.6-s disappearance, and the output rises again. However, the boost mode-enabled signal switches between high and low within a short time, starting from the time that v_O rises near to V_{com}. This is caused by the output voltage fluctuating around V_{com} in the process of rising.

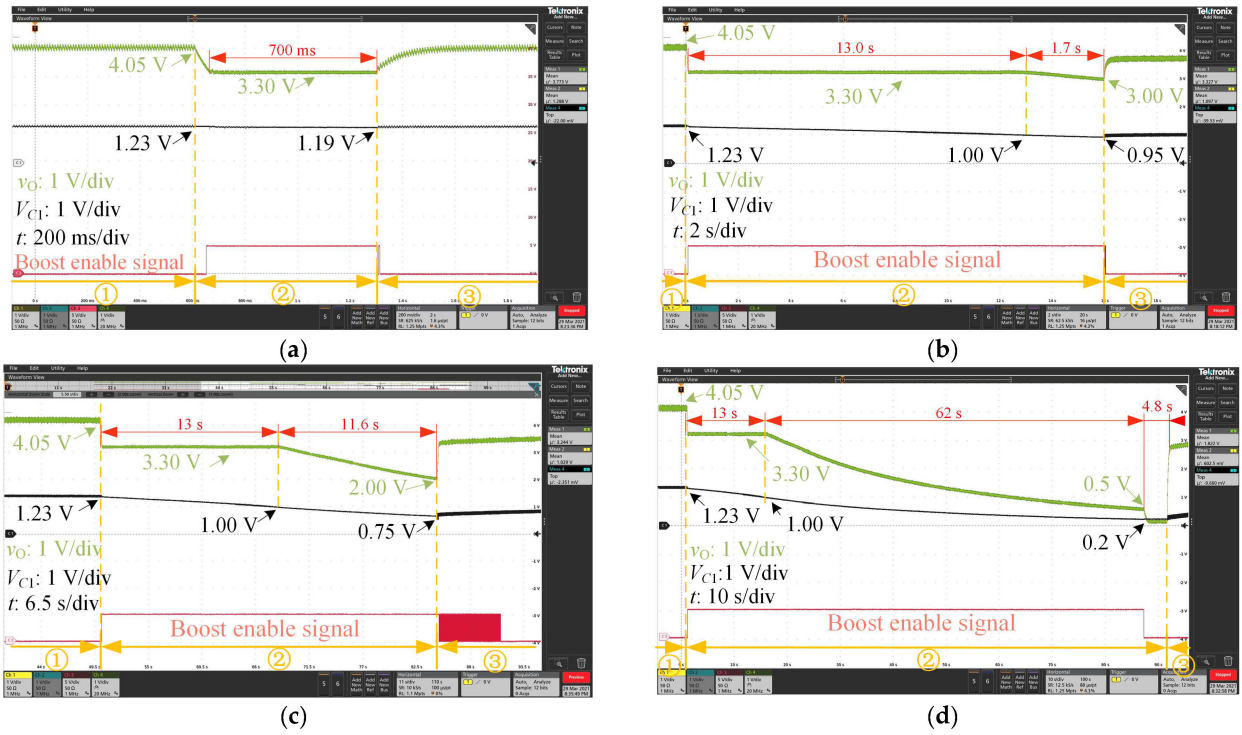

Figure 17. The mode transitions of the proposed dual-mode hybrid converter from the vibration's existence (①) to the vibration's disappearance (②), and to the resumption of the vibration (③). (**a**) the vibration is resumed after 700 ms of disappearance; (**b**) the vibration is resumed after 14.7 s of disappearance; (**c**) the vibration is resumed after 24.6 s of disappearance; (**d**) the vibration is resumed after 79.8 s of disappearance.

Case 4: As shown in Figure 17d, after the first 13 s of well regulation, v_O begins to drop. At 75 s, v_O drops to 0.5 V, which is lower than V_{hys-}, and the boost mode is shutdown. The vibration is resumed after 79.8 s disappearance, and the converter is restarted.

As depicted in Figure 17b–d, the time of voltage stabilization of the circuit is 13 s, which is 30% lower than the calculation results. This is because the large ESR (50 Ohms) of the selected super-capacitor consumes lots of stored energy in C_1.

Figure 18 shows the operation mode switches with the changes of external vibration. When the vibration disappears (e.g., region ②④⑥⑧), the boost-enabled signal becomes high. The circuit works under boost mode and the supercapacitor starts to discharge. v_O is stabilized at V_{O_boost} (3.3 V). When external vibration resumes (e.g., region ①③⑤⑦⑨), the output v_O starts to increase above V_{com} and the boost-enabled signal becomes low. The circuit switches back to VM mode and the supercapacitor voltage starts to rise. This shows that the circuit has a strong capability to maintain a stable output when the vibration is unstable. With an extra LDO stage, the output voltage can be better regulated.

Table 3 summarizes the performance of the proposed dual-mode hybrid step-up converter and compares it with state-of-art power converters in EVEH applications. Compared with active VM circuits [23,24] and direct AC~DC dual boost converters [12,14,25,26] where energy storages were not included, the proposed work has the advantage of continuously providing energy when the vibration disappears in a simple hybrid topology. In the meantime, it can achieve almost the same efficiency as a dual boost circuit with a much simpler control method. Some studies [16,18,27] adopted energy storage as the intermediate stage, as shown in Figure 2. The efficiencies of the topology given in [16,18] were lower than the proposed circuit due to the two-level transformation. One study [27] reported a high conversion efficiency of 85% and a stable output when the vibration source disappeared, but only simulation results were presented, and the output power was tens of orders lower than the proposed work. One study [19] described a three-port converter with additional

battery as the energy storage. A microcontroller was employed for MPPT control, which is quite power consuming and is not suitable for milli-power applications. The total efficiency was not reported in [19]. Furthermore, the state-of-arts in Table 3 all require extra start-up circuits, which may induce high energy loss with discrete components. Hence, the proposed dual-mode hybrid converter has been demonstrated to achieve a decent efficiency for EH energy conversion, and provides continuous output under unstable vibrations in a simple system architecture.

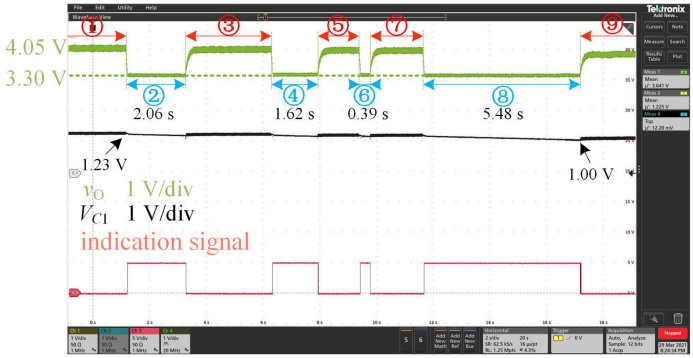

Figure 18. Key waveform of v_O, V_{C1} and the indication signal with the vibration status changes.

Table 3. Performance comparisons with state-of-art power conversions for vibration energy harvesting.

Topology	Stages of Converter	Output Voltage	Output Power	Maximum Efficiency	Control Mode	Uninterrupted Output ①	Extra Start-Up Circuit
Active Voltage-multiplier (n = 4) [23]	One	3.3 V	294 µW	80%	N/A	No	Yes
Cross-connected Active Voltage-multiplier (n = 1) [24]	One	2.68 V	960 µW	87% (Simulation)	N/A	No	Yes
Dual polarity Boost circuit [25]	One	3.3 V	50 mW	50%	Polarity detection + PWM	No	Yes
Dual Boost full-wave converter [14]	One	2.1 V	900 µW	65%	Burst + PWM	No	Yes
Dual Boost full-wave converter [26]	One	N/A	600 µW	89%	MPPT	No	Yes
Dual Boost split-capacitor converter [12]	One	3.3 V	21.8 mW	82.4%	COT	No	Yes
Voltage-multiplier + buck [18]	Two	2.57 V	500 µW	60%	MPPT	No	Yes
Full-wave Rectifier + step-down converter [16]	Two	3.3 V	104 mW	49%	N/A	Yes	Yes
Voltage-multiplier + boost [27]	Two	1 V	100 µW	85% (Simulation)	PWM	Yes	Yes
Dual Boost + Bi-directional Buck/Boost converter [19]	Two	3.3 V	10 mW	Not mentioned	MPPT + PWM	Yes	Yes
This work (n = 2)	**One**	**4.05 V**	**1.64 mW**	**60.7%**	**Mode switch + PWM**	**Yes**	**No**
Previous work [21] (n = 1)	**One**	**3.8 V**	**1.44 mW**	**85.9%**	**Mode switch + PWM**	**Yes**	**No**

① An energy storage element is included and can continue to supply power to the load when the source is disappeared.

7. Conclusions

A dual-mode hybrid step-up circuit with stable output for vibration energy harvesting (EH) was proposed in this paper. The converter operates as a multi-stage voltage multiplier when vibration exists, with the supercapacitor and output load both powered. Once vibration disappears, it will switch to boost mode, and the supercapacitor is employed as a power supply. The selections of the number of stages and supercapacitor are based on the voltage gain characteristics under different input and output impedance and the system's

energy utilization. A GaN HEMT-based dual-mode prototype was designed and tested with an in-house-designed EVEH device. Different operation modes were fully verified. When n = 2, the output voltage of the prototype reaches 4.05 V/1.64 mW in the existence of a vibration of 0.7 g and 100 Hz. The proposed converter is able to stabilize to 3.3 V in the absence of vibration for 13 s. The peak output efficiency of a hybrid circuit reaches 60.7%. The proposed hybrid converter has been demonstrated to achieve a descent efficiency for EH energy conversion, and provides continuous output under unstable vibrations in a simple system architecture without the need for an extra start-up circuit. It is a premium solution for a low-voltage, low-power EVEH system with unstable vibrations.

Future work will focus on the following two aspects. One is the low-voltage integration of the converter to reduce the loss brought about by discrete devices and parasitic interconnection. For example, the discrete Schottky diodes adopted in this paper suffer from high forward conduction because diodes with a voltage rating of 15 V and a current rating of 1 A are employed, which are far beyond the actual voltage and current requirements in the proposed application. Voltage/current-suitable devices will be available through IC integration, which will further improve the overall efficiency. The other focus is to apply the design of the energy harvester and hybrid step-up converter considering the specific vibration environment and load characteristics.

Author Contributions: Conceptualization, H.P. and J.Y.; methodology, J.Y.; software, J.Y.; validation, J.Y.; formal analysis, J.Y.; investigation, J.Y.; resources, H.P. and H.S.; data curation, J.Y.; writing—original draft preparation, J.Y.; writing—review and editing, H.P.; visualization, J.C.; supervision, C.Z.; project administration, H.P.; funding acquisition, H.P. All authors have read and agreed to the published version of the manuscript.

Funding: This research received no external funding.

Conflicts of Interest: The authors declare no conflict of interest.

References

1. Arnold, D.P. Review of Microscale Magnetic Power Generation. *IEEE Trans. Magn.* **2007**, *43*, 3940–3951. [CrossRef]
2. Khaligh, A.; Zeng, P.; Zheng, C. Kinetic Energy Harvesting Using Piezoelectric and Electromagnetic Technologies—State of the Art. *IEEE Trans. Ind. Electron.* **2010**, *57*, 850–860. [CrossRef]
3. Szarka, G.D.; Stark, B.H.; Burrow, S.G. Review of Power Conditioning for Kinetic Energy Harvesting Systems. *IEEE Trans. Power Electron.* **2012**, *27*, 803–815. [CrossRef]
4. Bai, Y.; Jantunen, H.; Juuti, J. Energy Harvesting Research: The Road from Single Source to Multisource. *Adv. Mater.* **2018**, *30*, 1707271. [CrossRef]
5. Tan, T.; Yan, Z.; Zou, H. Renewable energy harvesting and absorbing via multi-scale metamaterial systems for Internet of things. *Appl. Energy* **2019**, *254*, 113717. [CrossRef]
6. Jamadar, V.; Pingle, P.; Kanase, S. Possibility of harvesting Vibration energy from power producing devices: A review. In Proceedings of the International Conference on Automatic Control and Dynamic Optimization Techniques (ICACDOT), Pune, India, 9–10 September 2016; pp. 496–503.
7. Luo, W.; Cao, H.; Zhang, Z. Analysis of bridge vibration and noise caused by train crossing based on FE-SEA hybrid method. *J. East China Jiaotong Univ.* **2021**, *2*, 1–7.
8. Hou, W.; Li, Y.; Guo, W. Railway vehicle induced vibration energy harvesting and saving of rail transit segmental prefabricated and assembling bridges. *J. Clean. Prod.* **2018**, *182*, 946–959. [CrossRef]
9. Wang, X.; Chen, C.; Wang, N. A frequency and bandwidth tunable piezoelectric vibration energy harvester using multiple nonlinear techniques. *Appl. Energy* **2017**, *190*, 368–375. [CrossRef]
10. Rahimi, A.; Zorlu, Ö.; Muhtaroglu, A.; Kulah, H. Fully Self-Powered Electromagnetic Energy Harvesting System with Highly Efficient Dual Rail Output. *IEEE Sens. J.* **2012**, *12*, 2287–2298. [CrossRef]
11. Chen, J.; Peng, H.; Feng, Z.; Kang, Y. A GaN BCM AC–DC Converter for Sub-1 V Electromagnetic Energy Harvesting with Enhanced Output Power. *IEEE Trans. Power Electron.* **2021**, *36*, 9285–9299. [CrossRef]
12. Dayal, R.; Parsa, L. Low power implementation of maximum energy harvesting scheme for vibration-based electromagnetic microgenerators. In Proceedings of the Twenty-Sixth Annual IEEE Applied Power Electronics Conference and Exposition (APEC), Fort Worth, TX, USA, 6–11 March 2011; pp. 1949–1953.
13. Szarka, G.D.; Burrow, S.G.; Stark, B.H. Ultralow Power, Fully Autonomous Boost Rectifier for Electromagnetic Energy Harvesters. *IEEE Trans. Power Electron.* **2013**, *28*, 3353–3362. [CrossRef]

14. Belal, E.; Mostafa, H.; Ismail, Y.; Said, M.S. A voltage multiplying AC/DC converter for energy harvesting applications. In Proceedings of the 28th International Conference on Microelectronics (ICM), Cairo, Egypt, 17–20 December 2016; pp. 229–232.
15. Honda, M.; Sakurai, T.; Takamiya, M. Wireless temperature and illuminance sensor nodes with energy harvesting from insulating cover of power cords for building energy management system. In Proceedings of the IEEE PES Asia-Pacific Power and Energy Engineering Conference (APPEEC), Brisbane, Australia, 15–18 November 2015; pp. 1–5.
16. Itoh, G.; Tashiro, K.; Wakiwaka, H.; Kumada, T.; Okishima, K. Prototype of magnetic energy harvesting device as a 3.3 V battery. In Proceedings of the 11th International Symposium on Linear Drives for Industry Applications (LDIA), Osaka, Japan, 6–8 September 2017; pp. 1–4.
17. Cao, X.; Chiang, W.; King, Y.; Lee, Y. Electromagnetic Energy Harvesting Circuit with Feedforward and Feedback DC–DC PWM Boost Converter for Vibration Power Generator System. *IEEE Trans. Power Electron.* **2007**, *22*, 679–685. [CrossRef]
18. Tabesh, A.; Frechette, L.G. A Low-Power Stand-Alone Adaptive Circuit for Harvesting Energy from a Piezoelectric Micropower Generator. *IEEE Trans. Ind. Electron.* **2010**, *57*, 840–849. [CrossRef]
19. Wang, L.; Fu, M.; Wang, H. A three-port power electronic interface to harvest the maximum power in electromagnetic energy harvesting systems. In Proceedings of the IEEE 9th International Power Electronics and Motion Control Conference (IPEMC2020-ECCE Asia), Nanjing, China, 29 November–2 December 2020; pp. 1475–1481.
20. Wen, Y.; Shao, L.; Fernandes, R.; Trescases, O. Current-mode bi-directional single-inductor three-port DC-DC converter for portable systems with PV power harvesting. In Proceedings of the 15th European Conference on Power Electronics and Applications (EPE), Lille, France, 2–6 September 2013; pp. 1–10.
21. Yuan, J.; Peng, H.; Sun, H.; Xiao, H. A Single-Stage Dual-Mode AC-DC Converter for Vibration Energy Harvesting with Uninterrupted Output. In Proceedings of the 2021 IEEE Energy Conversion Congress and Exposition (ECCE), Virtual, 10–14 October 2021; pp. 5862–5866.
22. Sun, H.; Peng, H.; Chen, Y.; Xiao, H.; Liu, X.; Gao, K.; Wang, S.; Xu, P. A Compact Self-Power Module Based on Electromagnetic Energy Harvester and Voltage Multiplier. In Proceedings of the 2021 IEEE 4th International Electrical and Energy Conference (CIEEC), Wuhan, China, 28–30 May 2021; pp. 1–6.
23. Cheng, S.; Sathe, R.; Natarajan, R.D.; Arnold, D.P. A Voltage-Multiplying Self-Powered AC/DC Converter with 0.35-V Minimum Input Voltage for Energy Harvesting Applications. *IEEE Trans. Power Electron.* **2011**, *26*, 2542–2549. [CrossRef]
24. Rao, Y.; Arnold, D.P. An AC/DC voltage doubler with configurable power supply schemes for vibrational energy harvesting. In Proceedings of the 2013 Twenty-Eighth Annual IEEE Applied Power Electronics Conference and Exposition (APEC), Long Beach, CA, USA, 17–21 March 2013; pp. 2844–2851.
25. Mitcheson, P.D.; Green, T.C.; Yeatman, E.M. Power processing circuits for electromagnetic, electrostatic and piezoelectric inertial energy scavengers. *Microsyst. Technol.* **2007**, *13*, 1629–1635. [CrossRef]
26. Szarka, G.D.; Burrow, S.G.; Proynov, P.P.; Stark, B.H. Maximum Power Transfer Tracking for Ultralow-Power Electromagnetic Energy Harvesters. *IEEE Trans. Power Electron.* **2014**, *29*, 201–212. [CrossRef]
27. Liu, K.; Chen, M.; Gong, Y.; Fan, S.; Wang, G. A 100 μW AC-DC Boost Converter for Electromagnetic Energy Harvesting with 0.2 V Peak Self-starting Voltage and 85% Efficiency. In Proceedings of the 2018 IEEE Asia Pacific Conference on Circuits and Systems (APCCAS), Chengdu, China, 26–30 October 2018; pp. 493–496.